

Build Optimization of Fiber Reinforced Additively Manufactured Components

Aaditya Chandrasekhar · Tej Kumar · Krishnan Suresh

Abstract

Additive manufacturing (AM) has enabled fabrication of artifacts with unprecedented geometric and material complexity. The focus of this paper is on the build optimization of short fiber reinforced polymers (SFRP) AM components. Specifically, we consider optimization of the build direction, topology and fiber orientation of SFRP components. All the three factors have a significant impact on the functional performance of the printed part. While significant progress has been made on optimizing these independently, the objective of this paper is to consider all three factors simultaneously, and explore their interdependency, within the context of thermal applications.

Towards this end, the underlying design parameters are identified, appropriate sensitivity equations are derived, and a formal optimization problem is posed as an extension to the popular Solid Isotropic Material with Penalization (SIMP). Results from several numerical experiments are presented, highlighting the impact of build direction, topology and fiber orientation on the performance of SFRP components.

Keywords: Build optimization; fiber-reinforced; topology optimization; short fiber reinforced polymers

1 Introduction

Additive manufacturing (AM) has opened new opportunities to create parts with unprecedented geometric and material complexity. In AM, parts are fabricated layer-by-layer, as opposed to a subtractive process [18]. Fused deposition modeling (FDM) is one such AM process where a continuous thermoplastic (polymer) filament is deposited layer-by-layer (see Figure 1(a)). With continuously improving materials and technology, FDM is being used today to make functional parts for thermal and structural applications. For example, Figure 1(b) illustrates a heat exchanger where FDM's process capabilities are exploited to achieve large surface-to-volume ratio. Often, the structure can

Aaditya Chandrasekhar
Department of Mechanical Engineering
University of Wisconsin-Madison
E-mail: achandrasek3@wisc.edu

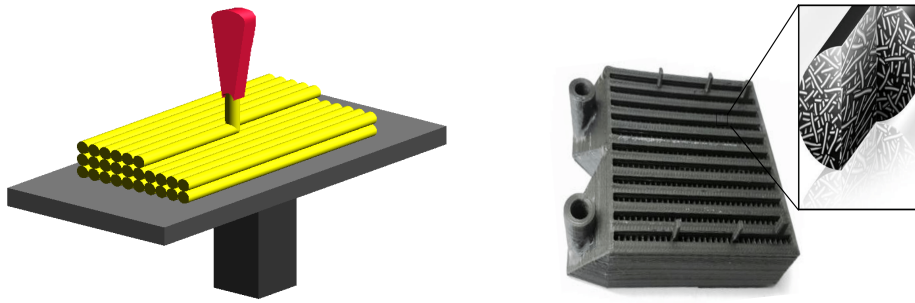
Tej Kumar
Department of Mechanical Engineering
University of Wisconsin-Madison
E-mail: tkumar3@wisc.edu

Krishnan Suresh
Department of Mechanical Engineering
University of Wisconsin-Madison
E-mail: ksuresh@wisc.edu

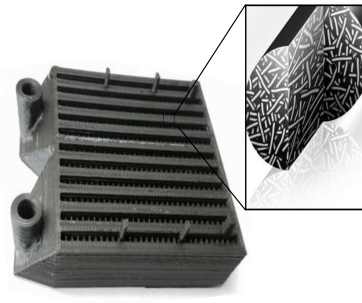
be optimized to reduce material consumption. Further, in such applications, to enhance performance, the polymer is often infused with short (typically, carbon) fibers [6] (Figure 1(c)). The functional properties of such short fiber reinforced polymers (SFRP) components depend significantly on the fiber distribution and orientation. These can be controlled in FDM by suitably modifying the raster path.

The focus of this paper is on the build optimization of such SFRP components. Specifically, the objective is to optimize the build direction, the topology and fiber orientation (raster path) for thermal applications. While significant progress has been made on each of these topics (for example, see [5] and [15]), the objective here is to consider all three factors simultaneously.

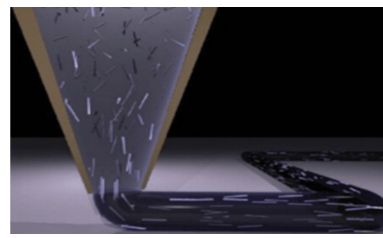
Towards this end, the remainder of this paper is organized as follows. The literature is reviewed with a motivating example in Section 2, and research gaps are identified. This is followed by a discussion on problem formulation, and derivation of sensitivity equations in Section 3. Results are discussed in Section 4, with a concluding note in Section 5.



(a) Illustration of the fused deposition modeling [45].



(b) A heat exchanger is printed using Carbon fiber reinforcement. This illustrates some of the recent advances in AM to print functional components. The image portrays the infill strategy used and the presence of fiber reinforcement in the polymer matrix.



(c) Polymers are filled with fibers to enhance mechanical properties [53]

Fig. 1 Fused Deposition Modeling of Fiber-Filled Composites.

2 Literature Review

As discussed in the previous section, the objective here is to simultaneously optimize the *build direction*, the *topology* and *fiber orientation*, to improve functional performance of SFRP parts. Prior work related to the above three build parameters is discussed next.

2.1 Build Direction

The build direction plays a significant role in the surface quality, print-time, and sacrificial support of FDM components; see [5], [12],[33], [28], [30],[54]. While these are important metrics, the current work focuses on the interplay between build direction and functional performance of the part. Specifically, it is well known that FDM introduces behavioral anisotropy [26], primarily due to incomplete fusion between adjoint layers. For example, consider Figure 2(a) where a heat load is applied on the top surface, and the temperature is fixed at the bottom. Figure 2(b) and Figure 2(c) illustrate two possible build directions. Observe that, in the former, the interlayer resistance is in the direction of heat flow, and is therefore not preferable, i.e., the build direction along X (or Y in this example) is preferable from a performance perspective. This simple example illustrates the importance of build direction on part performance. However, the optimal build orientation might not be obvious in many cases (see numerical examples). Researchers have proposed methods to optimize build direction for part performance. For example, Umetani [42] proposed a structural analysis technique based on a bending moment concept to optimize the build direction; however, isotropic material was assumed for simplicity, i.e., fiber reinforcement was not considered. On the other hand, material anisotropy was considered by Erva [41] where the build direction was optimized to maximize structural safety factor using a surrogate-optimization model.

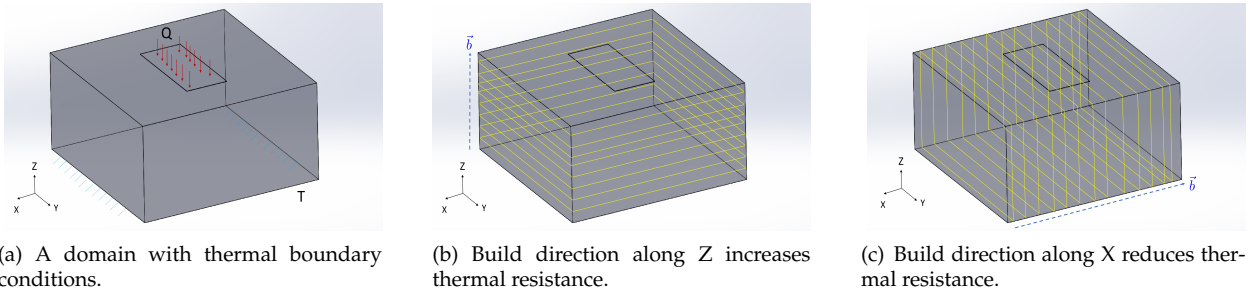


Fig. 2 Build orientation for optimizing functional performance of FDM.

2.2 Topology

With the advent of AM, there has been significant interest in optimizing the topology to improve part performance. For the above example, with X axis as the build direction, Figure 3 illustrates an optimal topology of 50% mass, compared to the original design, with minimal loss in performance. Various techniques such as Solid Isotropic Material with Penalization (SIMP) ([17], [3], [35]), level-set ([44]), Evolutionary Structural Optimization (ESO) ([48]), topological-sensitivity ([39]) may be employed for topology optimization. The limitation of prior work is that they assume a pre-defined build direction, and typically disregard material anisotropy (see [26] for exception).

Instead of optimizing the topology, researchers have also considered optimizing infill patterns. Martinez [25] proposed a stochastic method to generate compliant structures with a voronoi infill. Recently, Chougrani [9] suggested a lattice infill for AM. Wu et al. proposed a two-scale simultaneous optimization of shell-infill in the context of minimizing structural compliance [46]. Manufacturability of the model has been paid considerable consideration in works such as in [47] , [33] . Various attempts have been made to link micro-scale infill topology to the density values

obtained through optimization. *Multi-scale* optimization has been addressed in [52],[36],[49]. Recently, Dapogny [11] performed a 2D topology optimization considering specific infill patterns with anisotropic behavior.

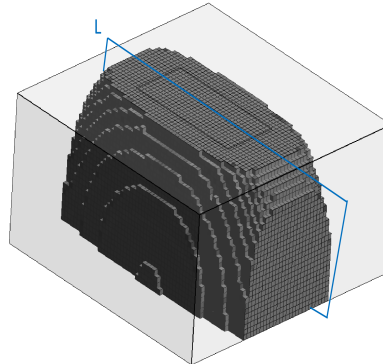


Fig. 3 The design shown in Figure 2(a) is optimized to 50 % of its initial volume.

The focus of this paper is on optimizing the topology, as opposed to finding an optimal infill pattern.

2.3 Fiber Orientation/Print Strategy

Finally, the print strategy can also have a significant impact on part performance, especially in the case of fiber reinforced polymers [4], since (1) fibers preferentially orient in the direction of extrusion of the filament from the print-nozzle [8], and (2) fibers add additional strength and thermal conductivity to the material [23]. Thus, an optimized fiber orientation/print-pattern as in Figure 4 can improve part performance. Towards this end, [34] recently introduced methods of achieving local site-specific control of fiber orientation. This coupled with development in multi-axis printing [10] paves new avenues to realize functionally tailored components with in-situ control of fiber composites. The problem of optimizing fiber orientation angle has been addressed within the context laminar composites. Discrete material optimization (DMO) is one of the most popular approaches, where a list of a priori directions (e.g. $0^\circ, \pm 45^\circ, \pm 90^\circ$) [37] is used. This avoids local minima, but can result in sub-optimal results. Interpolation schemes have also been suggested to overcome this limitation. Alternately, continuous fiber angle optimization (CFAO) has also been proposed [7]. This offers greater design freedom, but can result in a local minima. While the focus has been on laminar composites, there has been a recent increase in targeting these methodologies for AM. More references can be found at [43], [24],[2],[20],[19],[31].

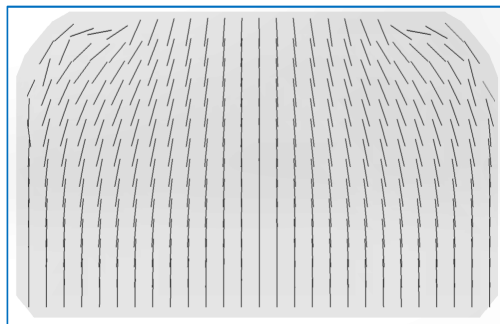


Fig. 4 Optimizing the print strategy can improve part performance.

2.4 Paper Contributions

The main contribution of this paper is a *comprehensive* approach to the build optimization of thermally loaded SFRP components by simultaneously considering the impact of build direction, print topology and fiber orientation. In particular, the proposed formulation is an extension to the popular SIMP method [35].

3 Problem Formulation

We start by discussing the design variables used in our formulation. This leads to a discussion on the optimization problem, sensitivity analysis, and proposed algorithm.

3.1 Design Parameters

Build Direction

Due to the incomplete fusion between subsequent layers of deposited material, the thermal conductivity tends to be lower in the direction of the build, leading to transversely isotropic properties. Prajapati [32] proposed to model the effective thermal conductivity along the build direction via

$$\frac{1}{k_z} = \frac{w_a + w_f}{w_a k_a + w_f k_f} + \frac{R_c}{L_h} \quad (1)$$

where k_z is the thermal conductivity in the build direction, k_a is the thermal conductivity of air, k_f is the thermal conductivity of the filament (with no fiber reinforcement), w_a is the air-gap between rasters, w_f is the width of the raster. R_c is the contact resistance between adjacent layers and L_h is the layer height. This is illustrated in Figure 5. Experimental studies show R_c to be in the order of $500 - 2000 [\mu\text{Km}^2\text{W}^{-1}]$ leading to $k_z/k_f \approx 0.6 - 0.8$. Similar decrease in mechanical properties have been reported by Knoop [21] and Farzadi [14]. Observe that the build-direction anisotropy is different from fiber induced anisotropy [53].

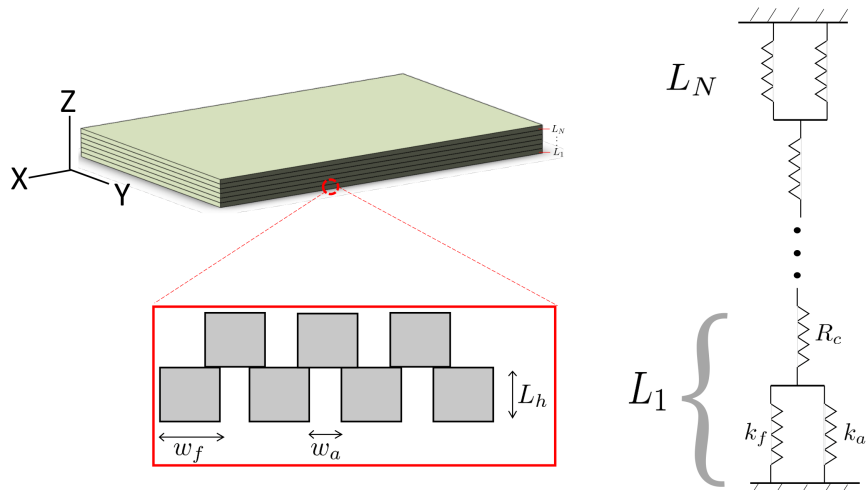


Fig. 5 Illustration showing thermal conductivity of a printed component.

In our formulation, we assume the part to have an initial build direction along the global Z-axis. We introduce *two* design parameters α_0 and β_0 as Eulerian angles to capture the rotation of the build direction about the global X and Y axis respectively via Equation (2). These two angle parameters are to be determined by the optimizer.

$$\mathbf{b} = R_x(\alpha_0)R_y(\beta_0)\mathbf{z} \quad (2)$$

where R_x and R_y are standard rotation matrices.

Topology

Next we consider the parameterization of topology. Here, the evolution of the topology is modeled using classic SIMP where each finite element e is assigned a density value $\rho_e \in [0, 1]$. A density value of one denotes the presence of material, and zero its absence. The density is further penalized by a constant p relating the material property via a power-law:

$$[K]_e = [K_0] + \rho_e^p ([\hat{K}] - [K_0]) \quad (3)$$

where $p = 3$, and $[k_0]$ is a small thermal conductivity assigned to void elements to prevent singularities.

Fiber Orientation

Next, we consider anisotropy due to fiber orientation. Mulholland [29] reported thermal anisotropy of specific SFRP materials (see Table 1). For example the baseline conductivity was reported to be $0.26[W/m - K]$ for PA6-CuF-20, significantly lesser than the fiber-infused counterpart. Here k_{\parallel} is the thermal conductivity achieved along the principal direction of the fibers, leveraging their higher conductivity and k_{\perp} can be attributed as the thermal conductivity imparted by the filament matrix. Since $k_{\perp}/k_{\parallel} \approx 0.13 - 0.38$, it is important to orient the fibers in an optimal fashion.

Material	$k_{\parallel}[W/(m - K)]$	$k_{\perp}[W/(m - K)]$
Onyx	0.88	0.30
PA6-CuF-20	4.84	0.76
PA6-CuF-25	5.52	0.77
RTP 0299 X 137152 C NAT/BLK	5.00	1.50
RTP 0299 X 137077 C NAT/BLK	18.01	4.50

Table 1 Thermal conductivity of a few SFRPs.

The finite element formulation used here (see later section) utilizes a geometrically congruent hexahedral (voxel) mesh. Thus, every finite element e is assigned an orientation angle θ_e , on a plane perpendicular to the build direction. This angle will be determined by the optimizer, and the resulting conductivity matrix can be expressed as:

$$[K]_e = R_{\mathbf{b}}(\theta_e) \hat{K} R_{\mathbf{b}}^T(\theta_e) \quad (4)$$

$$[\hat{K}] = \begin{bmatrix} k_{\parallel} & 0 & 0 \\ 0 & k_{\perp} & 0 \\ 0 & 0 & k_z \end{bmatrix} \quad (5)$$

where $[\hat{K}]$ is the thermal conductivity matrix along the principal directions assumed to be coincident with the global coordinates of the model. Combining the anisotropy due to layer-wise build (as discussed in the previous section) with that imparted by the fibers, we can see that $k_z/k_{\perp} \approx 0.08 - 0.31$. Further, $[R_b(\theta_e)]$ expresses the orientation of the infill fiber material with respect to the build direction.

Summary

Piecing all the design variables together, we have the effective conductivity given by:

$$[K]_e = [K_0] + \rho_e^p (R(\alpha_0, \beta_0, \theta_e)([\hat{K}] - [K_0])R(\alpha_0, \beta_0, \theta_e)^T) \quad (6)$$

where the rotation matrix is given by:

$$R(\alpha_0, \beta_0, \theta_e) = \begin{bmatrix} 1 & 0 & 0 \\ 0 \cos(\alpha_0) & -\sin(\alpha_0) \\ 0 \sin(\alpha_0) & \cos(\alpha_0) \end{bmatrix} \begin{bmatrix} \cos(\beta_0) & 0 & \sin(\beta_0) \\ 0 & 1 & 0 \\ -\sin(\beta_0) & 0 & \cos(\beta_0) \end{bmatrix} \begin{bmatrix} \cos(\theta_e) & -\sin(\theta_e) & 0 \\ \sin(\theta_e) & \cos(\theta_e) & 0 \\ 0 & 0 & 1 \end{bmatrix} \quad (7)$$

Observe that Equation 6 combines the effect of build direction (α_0 and β_0), fiber orientation (θ_e) and infill density (ρ_e), resulting in $2n + 2$ degrees of freedom where n is the number of finite elements.

3.2 Optimization Formulation

We are now ready to formulate the optimization problem. For a typical thermal problem, our objective is to minimize the thermal compliance (see [17],[16],[22],[13]), subject to a volume constraint:

$$\min_{\Omega \subset \Omega_0} C = \int_{\Omega} f \Theta d\Omega = \{\mathbf{f}\}^T \{\Theta\} \quad (8)$$

$$\text{s.t. } g(\rho) = \frac{\int \rho d\Omega}{V^*} - 1 \leq 0 \quad (9)$$

$$[\mathbf{K}]\{\Theta\} = \{\mathbf{f}\} \quad (10)$$

$$\alpha_0 \in [0, 2\pi] \quad (11)$$

$$\beta_0 \in [0, \pi] \quad (12)$$

$$\theta_e \in [0, 2\pi] \quad \forall e \quad (13)$$

$$\rho_e \in [0, 1] \quad \forall e \quad (14)$$

Observe that the system is governed by linear equations (10) derived from the finite element discretization of a steady state heat conduction problem. $[\mathbf{K}]$ is the stiffness matrix, $\{\Theta\}$ is the temperature field and $\{\mathbf{f}\}$ is the external

heat applied. V^* in Equation (9) refers to the final volume to be achieved upon optimization. The optimizer used here is the GCMMA [40]; this requires that the design variables be bounded. Thus, though the angular variables (namely α_0 , β_0 and θ_e) are periodic, and no bounds are required, limits are imposed as shown. The constraints for the build orientation is given by Equation (11) and (12). The constraint for fiber orientation is given by Equation (13) and Equation (14) sets the limit for density.

3.3 Sensitivity Analysis

In order to perform gradient based optimization, the sensitivity of the objective and constraints, with respect to the design variables is derived in this section.

Objective Sensitivity

Recall that the thermal compliance is given by:

$$\mathcal{C} = \{f\}^T \{\Theta\} \equiv \{\Theta\}^T [\mathbf{K}] \{\Theta\} \quad (15)$$

Differentiating Equation (15) with respect to a generic design variable x_i , we have,

$$\frac{\partial \{\mathcal{C}\}}{\partial x_i} = \frac{\partial \{\Theta\}}{\partial x_i}^T [\mathbf{K}] \{\Theta\} + \{\Theta\}^T \frac{\partial [\mathbf{K}]}{\partial x_i} \{\Theta\} + \{\Theta\}^T [\mathbf{K}] \frac{\partial \{\Theta\}}{\partial x_i} \quad (16)$$

Neglecting design-dependent loads we have, $\frac{\partial f}{\partial x_i} = \mathbf{0}$, Equation (10) is differentiated with respect to design variable x_i to get,

$$\frac{\partial \{\Theta\}}{\partial x_i} = -[\mathbf{K}]^{-1} \frac{\partial [\mathbf{K}]}{\partial x_i} \{\Theta\} \quad (17)$$

Inserting (17) into (16) results in:

$$\frac{\partial \{\mathcal{C}\}}{\partial x_i} = -\{\Theta\}^T \frac{\partial [\mathbf{K}]}{\partial x_i} \{\Theta\} \quad (18)$$

In particular, we have

$$\frac{\partial [\mathbf{K}]}{\partial \rho_e} = \iiint_{\Omega_e} [B]^T \frac{\partial [k]_e}{\partial \rho_e} [B] d\Omega_e \quad (19)$$

where $[B]$ is the gradient of the shape function matrix and,

$$\frac{\partial [k]_e}{\partial \rho_e} = p \rho_e^{p-1} ([R(\alpha_0, \beta_0, \theta_e)]([\hat{k}] - [k_0]) [R(\alpha_0, \beta_0, \theta_e)]^T) \quad (20)$$

Similarly, the sensitivity with respect to θ_e is given by:

$$\frac{\partial [\mathbf{K}]}{\partial \theta_e} = \iiint_{\Omega_e} [B]^T \frac{\partial [k]_e}{\partial \theta_e} [B] d\Omega_e \quad (21)$$

where,

$$\frac{\partial[k]_e}{\partial\theta_e} = \rho_e^p \left(\frac{\partial[R(\alpha_0, \beta_0, \theta_e)]}{\partial\theta_e} ([\hat{k}] - [k_0]) [R(\alpha_0, \beta_0, \theta_e)]^T + [R(\alpha_0, \beta_0, \theta_e)] ([\hat{k}] - [k_0]) \frac{\partial[R(\alpha_0, \beta_0, \theta_e)]^T}{\partial\theta_e} \right) \quad (22)$$

The sensitivity with respect to build orientation angle α_0 is given by,

$$\frac{\partial[\mathbf{K}]}{\partial\alpha_0} = \sum_e \iiint_{\Omega_e} [\mathbf{B}]^T \frac{\partial[k]_e}{\partial\alpha_0} [\mathbf{B}] d\Omega_e \quad (23)$$

where $\frac{\partial[k]_e}{\partial\alpha_0}$ follows an expression similar to that of Equation (22). The sensitivity with β_0 follows suit with α_0 and is omitted here for sake of brevity. Further, we note the highly coupled nature of the different design variables and the interplay between density, fiber directions and build orientation in determining the objective and sensitivities, thus strengthening the argument for the need of a coupled solver.

Note that the sensitivity with respect to the build orientation angles (Equation (23)) is summed over all elements. This is in contrast to sensitivity with respect to infill densities (Equation (20)) and fiber orientation (Equation (21)). In other words, build orientation is global, while infill density and fiber orientation apply to each element.

Constraint Sensitivity

The global volume constraint (Equation (9)) in the discrete form can be expressed as,

$$\frac{\sum_e \rho_e v_e}{V^*} - 1 \leq 0 \quad (24)$$

Where v_e is the volume of a discrete element in the congruent hexahedral voxel mesh. The gradient of the global volume constraint with density can be obtained as,

$$\frac{\partial g}{\partial \rho_e} = \frac{v_e}{V^*} \quad (25)$$

The sensitivity is zero with respect to θ_e , α_0 , and β_0 . The box-constraints limiting the range of the design variables given by Equations (11), (12), (13) and (14) are considered implicitly by the globally convergent method of moving asymptotes (GCMMA) solver used in this paper [40]. While any finite element solver can be used, an in-house assembly-free solver [27], [51] is employed here.

3.4 Optimization Algorithm

The optimization algorithm utilizes GCMMA [40] to optimize and an in-house assembly free finite element solver to perform the FEA [50]. The algorithm followed is described below (Algorithm 1):

4 Numerical Experiments

We now demonstrate the proposed method through several examples. The examples considered, and the corresponding sub-sections, are summarized in Table 2. For example, in sub-section 4.1.1, we optimize just the topology,

Algorithm 1 Build, Infill and Fiber Optimization

```

1: procedure BUILDOPT( $V_c$ )                                ▷ Max. Vol. Frac.  $V_c \in [0, 1]$ 
2:    $i = 0$                                               ▷ Iteration Index
3:    $\phi = \{\bar{\rho}, \bar{\theta}, \alpha_0, \beta_0\}$           ▷ Opt. Variables
4:    $\Delta = 1.0$                                          ▷ Design Change
5:   while  $\Delta > \epsilon$  and  $i \leq \text{MaxIter}$  do
6:      $i \leftarrow i + 1$ 
7:      $[K] \leftarrow (\phi)$                                ▷ via Eq. 6
8:      $\{\Theta\} \leftarrow [K]^{-1}\{f\}$                   ▷ Deflated-Preconditioned Assembly-Free solver
9:      $C \leftarrow (\{\Theta\}, \{f\})$                       ▷ via Eq. 15
10:     $g \leftarrow (\bar{\rho}, V^*)$                          ▷ Vol. Constraint Eq.24
11:     $(\frac{\partial C}{\partial \rho_e}, \frac{\partial C}{\partial \theta_e}, \frac{\partial C}{\partial \alpha_0}, \frac{\partial C}{\partial \beta_0}, \frac{\partial g}{\partial \rho_e})$  ▷ via Eq. 20,22,23, 25
12:     $\phi^i \leftarrow (C, g, \frac{\partial C}{\partial \rho_e}, \frac{\partial C}{\partial \theta_e}, \frac{\partial C}{\partial \alpha_0}, \frac{\partial C}{\partial \beta_0}, \frac{\partial g}{\partial \rho_e})$  ▷ GCMMA Solver [40]
13:     $\Delta = (|\phi_e^i - \phi_e^{i-1}|)$ 

```

by assuming a fixed build direction and fixed fiber orientation. Similarly, in sub-section 4.1.2, we optimize just the fiber orientation, by assuming a fixed build direction, fixed and topology, and so on. The examples were chosen to highlight the importance of one or more design variables. All experiments were conducted on a desktop PC equipped with an Intel-i7 12-core processor with 32 GB RAM running at 3.2 GHz.

Section	Build Dir	Fiber Orient.	Topology
4.1.1	✗	✗	✓
4.1.2	✗	✓	✗
4.1.3	✗	✓	✓
4.2 , 4.3	✓	✗	✓
4.4	✓	✓	✓

Table 2 Summary of various examples considered.

4.1 Fixed Build Orientation

In this section, the build orientation is assumed to be fixed, while the topology and/or the fiber orientation are optimized.

4.1.1 Optimization of topology

Consider a plate, with a thickness of 0.5 mm, illustrated in Figure 6. The thermal boundary conditions are applied as illustrated in Figure 6, where $T = 0^\circ\text{C}$, and the heat flux $Q = 10^4 [\text{W}/\text{m}^2]$. The build direction is along the thickness direction. Further, in this subsection, the material is assumed to be isotropic with $k = 0.77 [\text{W}/\text{m}\cdot\text{K}]$, and therefore the fiber orientation is not relevant. The only design variables are the SIMP densities; the thermal compliance must be minimized for a target volume fraction of 0.5. For finite element analysis, the domain is discretized into 25,000 hexahedral elements (voxels).

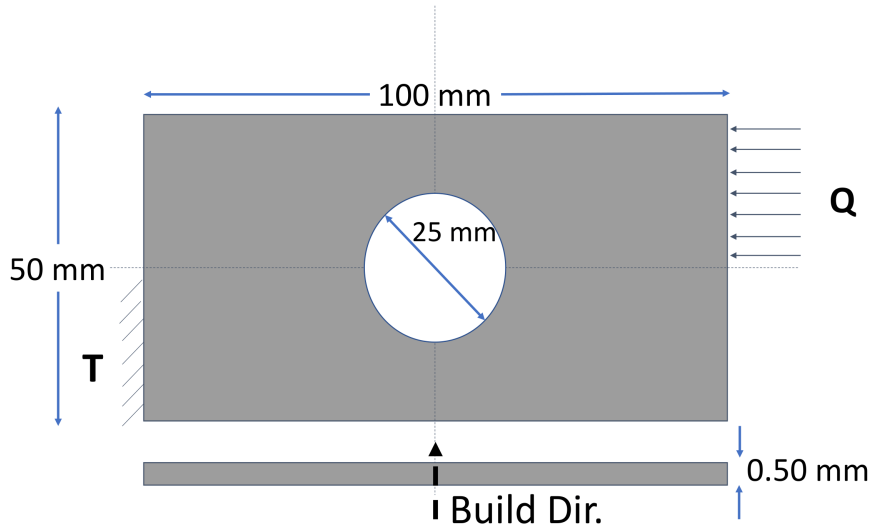


Fig. 6 Illustration of a plate problem with thermal boundary conditions.

To optimize the topology, all elements are assigned an initial density of 0.5 (the target volume fraction). The optimization algorithm described earlier is now exploited to find the optimal topology that minimizes the thermal compliance. The optimization terminates when the relative change in the thermal compliance is less than 10^{-4} . The final topology, together with the convergence, is illustrated in Figure 7; observe that the topology aligns with the flow of heat, as expected. The solver completed the optimization in 27 iterations, taking a total time of 3.27 min.

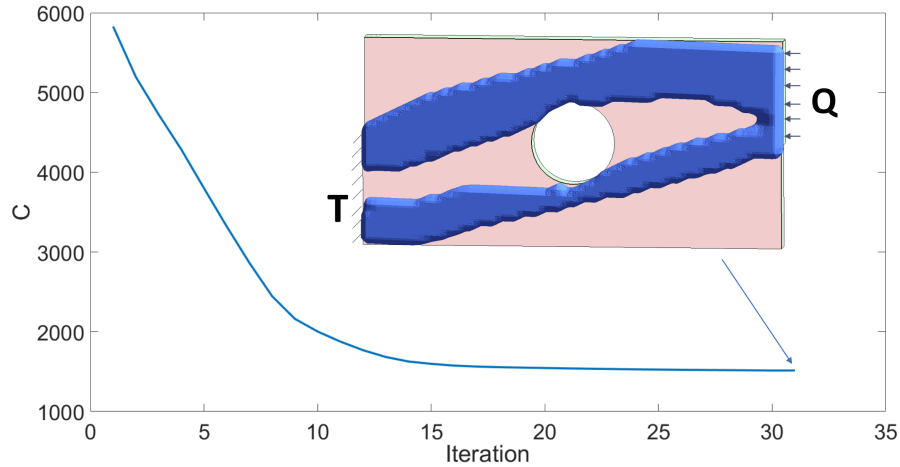


Fig. 7 Topology and convergence plot for plate problem.

4.1.2 Fiber Optimization

Next, we consider optimizing just the fiber orientation for the above example; the build direction is fixed as before, and the topology is not optimized, i.e., 100% volume. The material is assumed to be PA6-CuF-25 (see Table 1); the anisotropic conductivity is an impetus for preferential fiber orientation. All elements are initially oriented with $\theta_e =$

0° . After optimization, Figure 8 illustrates convergence and the orientation of the fibers. The solver completed the optimization in 20 iterations, taking a total time of 2.81 min.

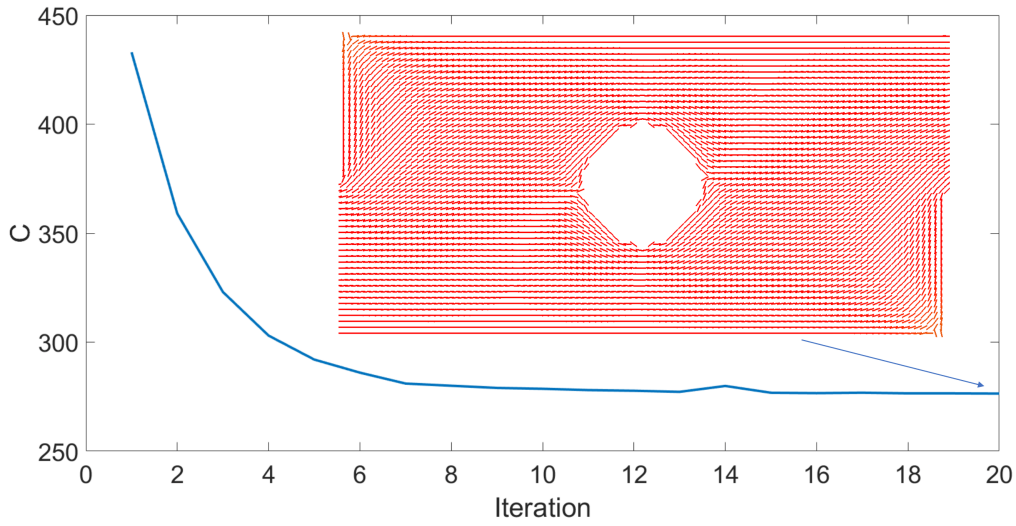


Fig. 8 Fiber orientation and convergence plot for plate problem.

4.1.3 Fiber and Topology Optimization

Next, we combine fiber and topology optimization for the above example. All elements have an initial density of 0.5, and the fibers are oriented at $\theta = 0^\circ$. Figure 9 illustrates the convergence, and the resulting topology, with fiber orientation. We observe a significant improvement in performance, compared to only optimizing the topology (section 4.1.1), or the fibers (section 4.1.2). The solver completed the optimization in 50 iterations, taking a total time of 4.15 min.

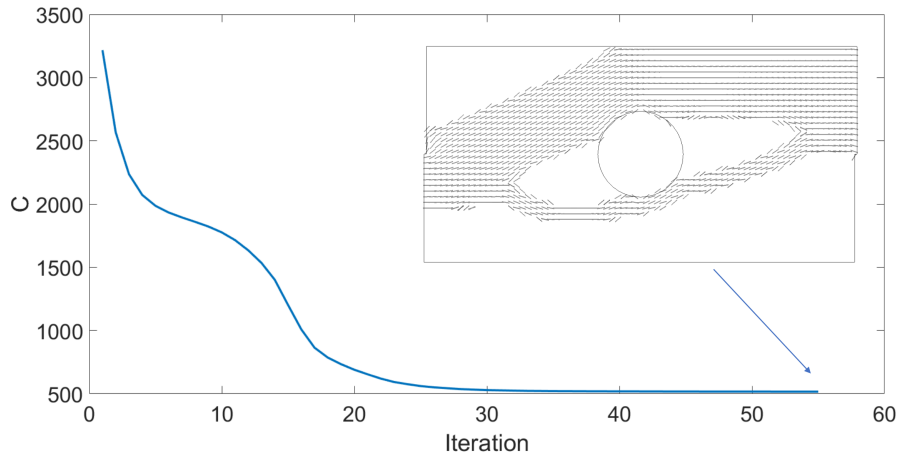


Fig. 9 Fiber orientation and convergence plot for 2D plate problem.

4.2 Build Orientation and Topology Optimization

We now illustrate an example where the benefits of optimizing the build direction becomes evident. Consider the geometry in Figure 10, where $T = 0^\circ\text{C}$ on the (a subset of the) top face, and a heat flux of 10^3 W/m^2 is applied on the bottom face. The material is assumed to be isotropic, i.e., fiber orientation is disregarded. However, observe that depending on the build direction, inter-layer anisotropy will be induced. For example, if the build direction is along Z-axis, then $k_x = k_y = 0.76 \text{ [W/m-K]}$ while $k_z = 0.45 \text{ [W/m-K]}$. For finite element analysis, the domain was meshed with 100,000 elements.

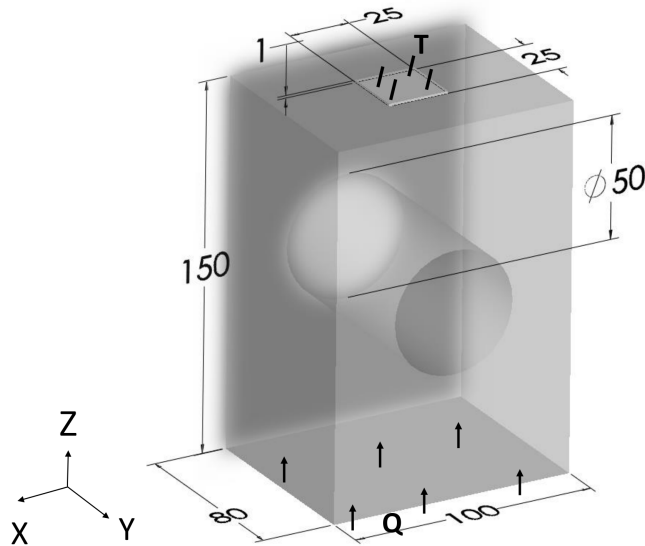


Fig. 10 A box-geometry with a center hole, and associated boundary conditions; all dimensions in mm.

To isolate the impact of build direction, two sets of optimization studies were carried out. In the first set, the build direction was fixed along Z-axis; observe that this is sub-optimal since the heat sink and source are separated along the Z-axis. The topology was then optimized for 3 different volume fractions: 30%, 50% and 75%. The final compliances, and time taken, are reported in the second column of Table 3. In the second set, the build-direction was also optimized (with an initial guess along Z-axis). The thermal compliance, together with the optimal build-direction and time taken are reported in the third column; the optimal build direction is approximately along X-axis. As one can observe, the compliance reduces significantly when the build direction is optimized.

Volume Fraction (%)	Fixed Build Dir. $\mathbf{b} = \{0, 0, 1\}$		Optimized Build Dir.		
	C	t	C	\mathbf{b}	t
30	C = 13.2	t = 12.2 mins	C = 4.54	$\mathbf{b} = \{0.93, 0.27, 0.24\}$	t = 18.1 mins
50	C = 4.33	t = 9.1 mins	C = 1.56	$\mathbf{b} = \{0.97, 0.21, 0.12\}$	t = 14.3 mins
75	C = 2.42	t = 6.7 mins	C = 1.00	$\mathbf{b} = \{0.96, 0.24, 0.14\}$	t = 11.2 mins

Table 3 Compliances, computational time with and without build direction optimization.

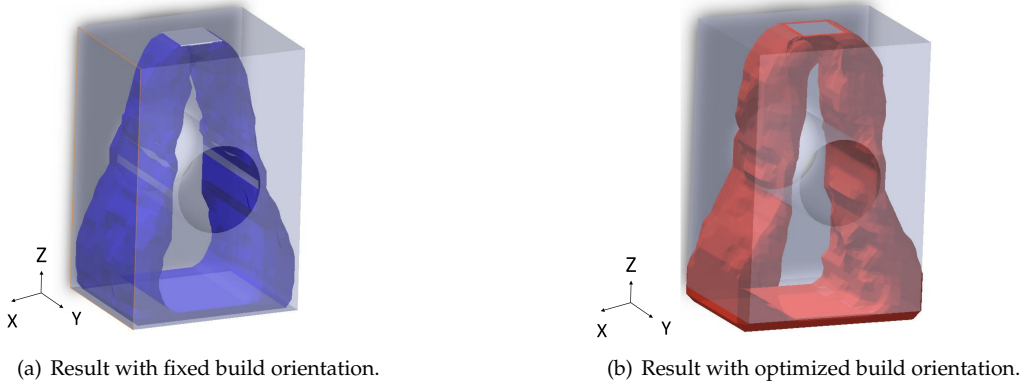


Fig. 11 Topologies at 30% volume fraction for fixed and optimized build orientation.

4.3 Sequential vs. Simultaneous Optimization

In this example, we illustrate the strong interplay between the three sets of design parameters. Consider the geometry and thermal boundary conditions illustrated in Figure 12, with $Q = 10,000[W/m^2]$ and $T = 0^\circ C$. As before, we set $k_{\parallel} = k_{\perp} = 0.76[W/m - K]$ and $k_z = 0.45[W/m - K]$. The domain was meshed with 10,000 elements, and the target volume fraction was 0.5. We consider here three optimization scenarios. In the first scenario, we first optimize the build orientation (for full volume), and then optimize the topology and fiber orientation, using the computed build direction. In the second scenario, the build direction and topology are optimized simultaneously, following which the fiber orientation is optimized. Finally, in the third scenario, all three (build, topology and fiber orientation) are simultaneously optimized.

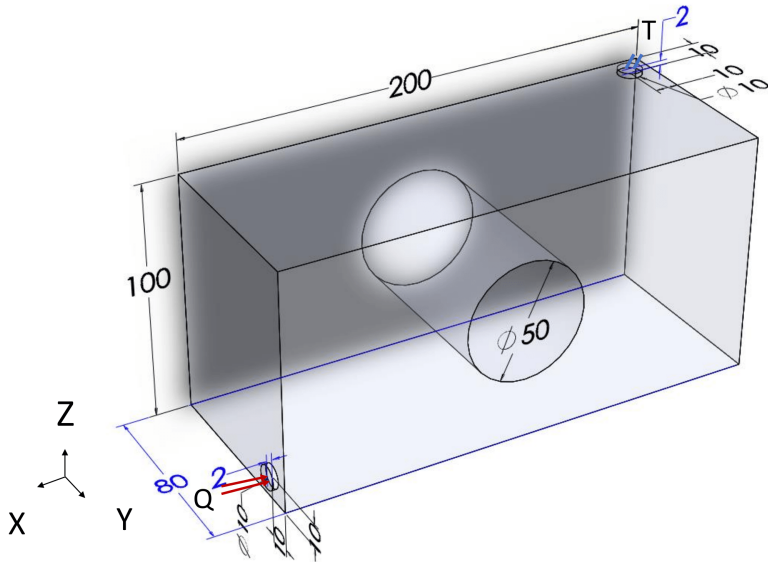
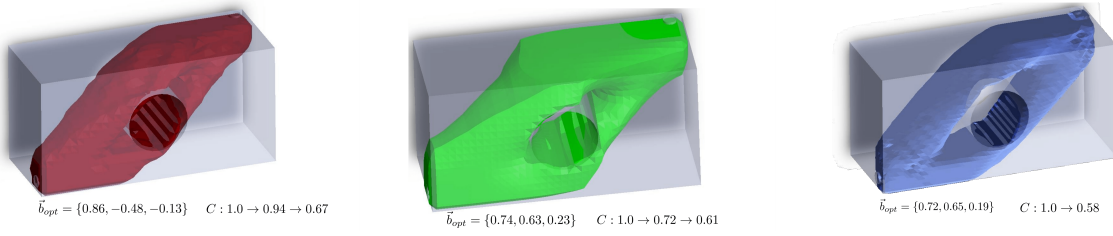


Fig. 12 Geometry and boundary conditions to compare sequential and simultaneous optimization.

The resulting designs are presented in Figure 13(a), 13(b) and 13(c) respectively. The topologies exhibit minor differences, but the optimal build directions are significantly different. Further, in the first scenario, the relative compliance dropped to 0.94 (after optimizing just the build direction taking 23 CG iterations), and then to 0.67 (after optimizing the topology and fiber with 62 CG Iterations), taking a total of 85 CG iterations. In the second scenario, the

relative compliance dropped to 0.72 (showcasing the effect of build and topology) which then reduced to 0.61 after 41 and 37 CG iterations respectively, totaling to 78 iterations. Finally, optimizing all three variables simultaneously results in the lowest compliance of 0.58 after 91 CG iterations. Comparing the final compliance of 13(b) and 13(c) we note that the combined optimization consumes about 16% more iterations for about 6% gain in performance. This can be attributed to the oscillatory behavior in the convergence of the optimizer and the subjective nature of the problem.



(a) Build → Topology and fiber optimization (b) Build and topology → Fiber optimization (c) Simultaneous optimization of Build, fiber and topology.

Fig. 13 Comparison of sequential and simultaneous optimization.

4.4 Complete Optimization

In this section, we highlight the full potential of the solver by simultaneously optimizing the build direction, topology, fiber orientation, for the geometry in Figure 14. The prescribed boundary conditions are a fixed temperature of 0°C and a heat flux of $10^4 \text{ [W/m}^2\text{]}$. We assume the material be PA6-CuF-25 (Table 1) with $k_z = 0.45 \text{ [W/m-K]}$. The desired volume fraction is 0.3. The design is discretized with 50,000 elements. As before, the initial density of all the elements is 0.3 (desired volume fraction), the orientation of the fibers is 0° . Several instances of optimization were executed using different initial build orientation; the results are tabulated in Table 4. While the final build direction is almost identical in each case (upto a sign), the final compliances are slightly different. This reflects the sensitivity of the compliance to the build direction.

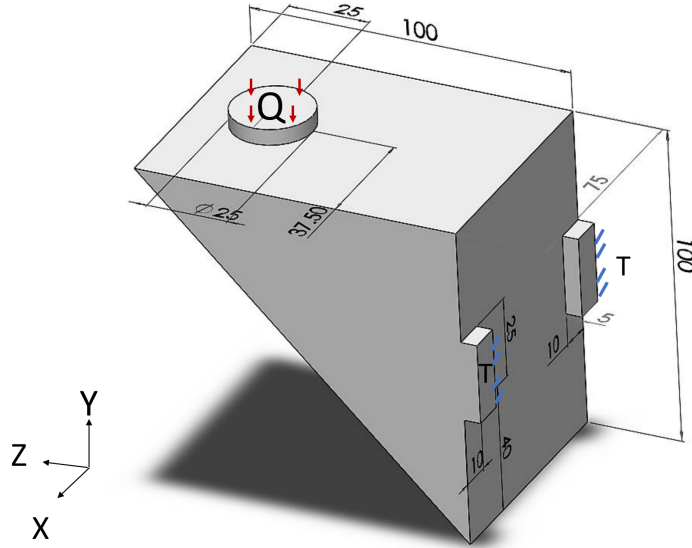


Fig. 14 A triangular block with boundary conditions.

The optimal topology and build direction are illustrated in Figure 15.

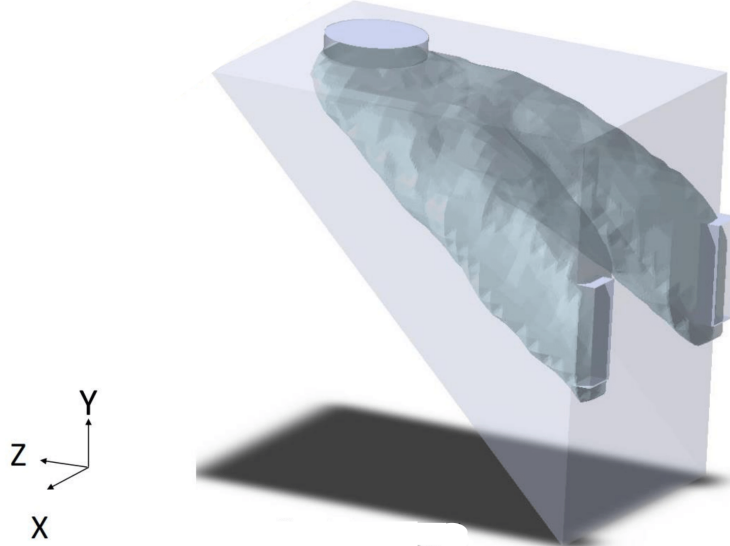


Fig. 15 The final topology and build direction upon optimization.

Trial	\mathbf{b}_{init}	\mathbf{b}_f	C_0	C_f
1	$\{1, 0, 0\}$	$\{0.773, 0.63, 0.006\}$	19813	803
2	$\{0, 1, 0\}$	$\{-0.773, -0.634, -0.0019\}$	38059	823
3	$\{0, 0, 1\}$	$\{-0.776, 0.63, 0.002\}$	43945	858
4	$\{1/\sqrt{2}, -0.5, 0.5\}$	$\{0.773, -0.63, 0.0037\}$	22491	873

Table 4 Impact of initial build direction on the optimal build direction and compliance.

The compliance convergence (for the fourth build orientation scenario) is plotted in Figure 16, together with the optimal fiber orientation for one of the cross-sections. We observe a sharp decrease in the compliance near the 20th iteration; this can be attributed to the convergence in the build orientation.

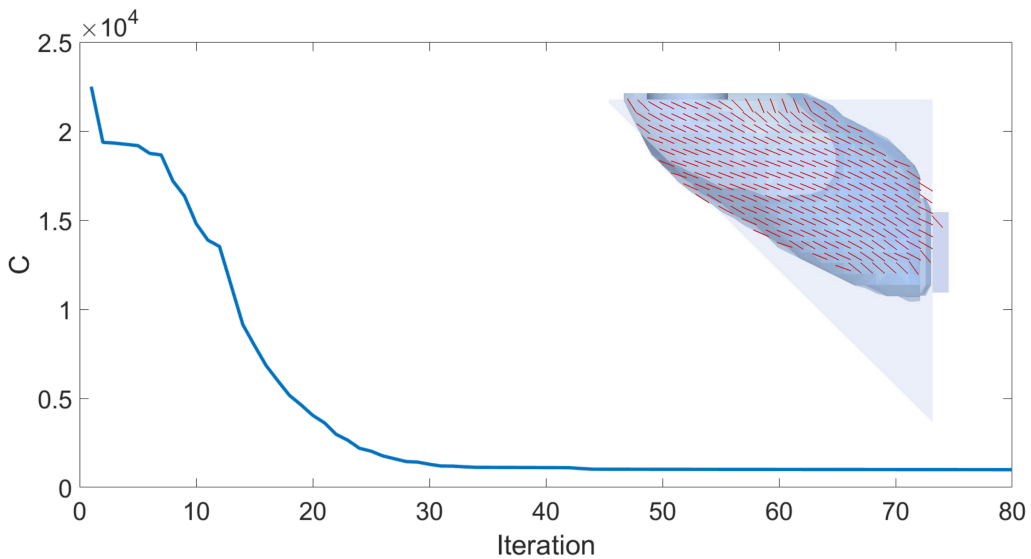


Fig. 16 The evolution of compliance with iteration. The final topology along with orientation of the fiber at a cross section is shown.

The convergence of the build direction is illustrated in Figure 17. We observe that the optimizer considers various orientations to finally arrive at the optimal. Further, we notice that the convergence of the orientation is non-smooth. We conjecture that the oscillatory nature is due the strong interplay between the build orientation and the evolving topology / fiber orientation. The solver completed the optimization in 80 iterations taking a total time of 38.5 min.

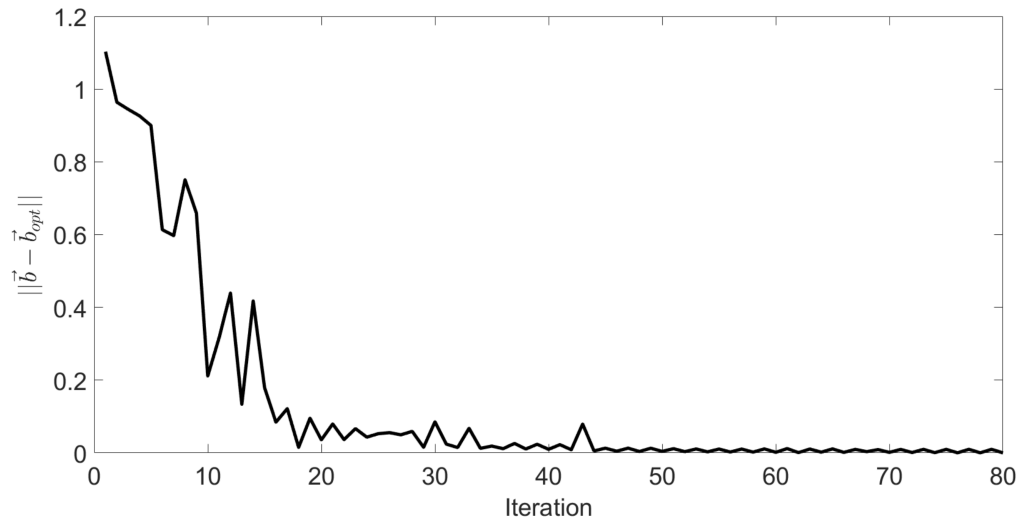


Fig. 17 The convergence of the norm of the difference between the optimal build vector and that at given iteration.

5 Replication of Results

The paper uses the Pareto code, developed at UW-Madison, that has been assigned to Wisconsin Alumni Research Foundation (WARF). Due to restrictions imposed by WARF, we are unable to provide public access to this software for replication of results.

6 Conclusion

The main contribution of this paper is an integrated framework for the simultaneous optimization of build direction, topology and fiber orientation of SFRP components. The numerical experiments demonstrated that all three factors must be considered for optimal performance. A global volume constraint was imposed to drive the optimizer towards minimizing compliance. The layer-wise printing paradigm of AM was of central focus, and methods were proposed to include the consequence of anisotropic material properties.

There are several areas for future research. The present formulation does not include several AM-constraints such as overhang surfaces, minimum feature size, surface finish, etc. Further post-processing [1] might be required to produce smooth transitions in fiber orientation. Generation of machine instructions from the obtained topology and orientation field is also a topic of future research [38].

Acknowledgments

The information, data, or work presented herein was funded in part by the Advanced Research Projects Agency-Energy (ARPA-E), U.S. Department of Energy, under Award Number DE-AR0000573, National Science Foundation (NSF) under Award NSF-1561899. The views and opinions of authors expressed herein do not necessarily state or reflect those of the United States Government or any agency thereof. Prof. Suresh is a consulting Chief Scientific Officer of SciArt, Corp, which has licensed the Pareto technology (for its finite element capabilities), developed in Prof. Suresh's lab, through Wisconsin Alumni Research Foundation.

References

1. Grégoire Allaire, Perle Geoffroy-Donders, and Olivier Pantz. Topology optimization of modulated and oriented periodic microstructures by the homogenization method. *Computers & Mathematics with Applications*, Aug 2018.
2. M. P. Bendsoe, J. M. Guedes, R. B. Haber, P. Pedersen, and J. E. Taylor. An Analytical Model to Predict Optimal Material Properties in the Context of Optimal Structural Design. *Journal of Applied Mechanics*, 61(4):930, dec 2008.
3. M P Bendsoe and Ole. Sigmund. *Topology optimization: theory, methods, and applications*. Springer Berlin Heidelberg, 2 edition, 2003.
4. L. G. Blok, M. L. Longana, H. Yu, and B. K.S. Woods. An investigation into 3D printing of fibre reinforced thermoplastic composites. *Additive Manufacturing*, 22:176–186, Aug 2018.
5. A. Boschetto and L. Bottini. Accuracy prediction in fused deposition modeling. *The International Journal of Advanced Manufacturing Technology*, 73(5-8):913–928, Jul 2014.
6. E. C. Botelho, Figiel, M. C. Rezende, and B Lauke. Mechanical behavior of carbon fiber reinforced polyamide composites. *Composites Science and Technology*, 63(13):1843–1855, Oct 2003.
7. Christopher J Brampton, K Chauncey Wu, and H Alicia Kim. New optimization method for steered fiber composites using the level set method. *Structural and Multidisciplinary Optimization*, 52(3):493–505, 2015.
8. Bastian Brenken, Eduardo Barocio, Anthony Favaloro, Vlastimil Kunc, and R Byron Pipes. Fused filament fabrication of fiber-reinforced polymers: A review. *Additive Manufacturing*, 21:1–16, May 2018.
9. Laurent Chougrani, Jean Philippe Pernot, Philippe Véron, and Stéphane Abed. Lattice structure lightweight triangulation for additive manufacturing. *CAD Computer Aided Design*, 90:95–104, Sep 2017.
10. Chengkai Dai, Charlie CL Wang, Chenming Wu, Sylvain Lefebvre, Guoxin Fang, and Yong-Jin Liu. Support-free volume printing by multi-axis motion. *ACM Transactions on Graphics (TOG)*, 37(4):134, 2018.

11. Charles Dapogny, Rafael Estevez, Alexis Faure, and Georgios Michailidis. Shape and topology optimization considering anisotropic features induced by additive manufacturing processes. *Computer Methods in Applied Mechanics and Engineering*, 344:626–665, 2019.
12. Paramita Das, Ramya Chandran, Rutuja Samant, and Sam Anand. Optimum Part Build Orientation in Additive Manufacturing for Minimizing Part Errors and Support Structures. In *Procedia Manufacturing*, volume 1, pages 343–354. Elsevier, Jan 2015.
13. Shiguang Deng and Krishnan Suresh. Multi-constrained topology optimization via the topological sensitivity. *Structural and Multidisciplinary Optimization*, 51(5):987–1001, May 2015.
14. Arghavan Farzadi, Mehran Solati-Hashjin, Mitra Asadi-Eydivand, and Noor Azuan Abu Osman. Effect of layer thickness and printing orientation on mechanical properties and dimensional accuracy of 3D printed porous samples for bone tissue engineering. *PLoS ONE*, 9(9):e108252, 2014.
15. Miguel Fernandez-Vicente, Wilson Calle, Santiago Ferrandiz, and Andres Conejero. Effect of Infill Parameters on Tensile Mechanical Behavior in Desktop 3D Printing. *3D Printing and Additive Manufacturing*, 3(3):183–192, Sep 2016.
16. T Gao, W H Zhang, J H Zhu, Y J Xu, and D H Bassir. Finite Elements in Analysis and Design Topology optimization of heat conduction problem involving design-dependent heat load effect. *Finite Elements in Analysis and Design*, 44:805–813, 2008.
17. Allan Gersborg-Hansen, Martin P Bendsøe, and Ole Sigmund. Topology optimization of heat conduction problems using the finite volume method. *Structural and multidisciplinary optimization*, 31(4):251–259, 2006.
18. I. Gibson, D. W. Rosen, and B. Stucker. *Additive manufacturing technologies: Rapid prototyping to direct digital manufacturing*. Springer, New York, 2010.
19. Zafer Gürdal, Raphael T. Haftka, and Prabhat Hajela. *Design and optimization of laminated composite materials*. Wiley, 1999.
20. J. Huang and R. T. Haftka. Optimization of fiber orientations near a hole for increased load-carrying capacity of composite laminates. *Structural and Multidisciplinary Optimization*, 30(5):335–341, nov 2005.
21. F Knoop and V Schoeppner. Mechanical and Thermal Properties of Fdm Parts Manufactured With Polyamide 12. *Solid Freeform Fabrication Symposium*, pages 935–948, 2015.
22. Qing Li, Grant P. Steven, Osvaldo M. Querin, and Y. M. Xie. Shape and topology design for heat conduction by Evolutionary Structural Optimization. *International Journal of Heat and Mass Transfer*, 42(17):3361–3371, Sep 1999.
23. Jikai Liu, Andrew T Gaynor, Shikui Chen, Zhan Kang, Krishnan Suresh, Akihiro Takezawa, Lei Li, Junji Kato, Jinyuan Tang, Charlie CL Wang, et al. Current and future trends in topology optimization for additive manufacturing. *Structural and Multidisciplinary Optimization*, pages 1–27, 2018.
24. Jian Hui Luo and Hae Chang Gea. Optimal bead orientation of 3D shell/plate structures. *Finite Elements in Analysis and Design*, 31(1):55–71, nov 1998.
25. Jonàs Martínez, Jérémie Dumas, and Sylvain Lefebvre. Procedural Voronoi Foams for Additive Manufacturing. *ACM Transactions on Graphics*, 35(4):12, Jul 2016.
26. Amir M. Mirzendehdel, Behzad Rankouhi, and Krishnan Suresh. Strength-based topology optimization for anisotropic parts. *Additive Manufacturing*, 19:104–113, Jan 2018.
27. Amir M. Mirzendehdel and Krishnan Suresh. A Deflated Assembly Free Approach to Large-Scale Implicit Structural Dynamics. *Journal of Computational and Nonlinear Dynamics*, 10(6):061015, Nov 2015.
28. Omar A Mohamed, Syed H. Masood, and Jahar L Bhowmik. Optimization of fused deposition modeling process parameters: a review of current research and future prospects. *Advances in Manufacturing*, 3(1):42–53, 2015.
29. Thomas Mulholland, A Falke, and Natalie Rudolph. Filled Thermoconductive Plastics for Fused Filament Fabrication. In *Solid Freeform Fabrication*, pages 871–883, Austin, TX, 2016.
30. A Sanati Nezhad, F Barazandeh, A R Rahimi, and M Vatani. Pareto-Based Optimization of Part Orientation in Stereolithography. *Proceedings of the Institution of Mechanical Engineers, Part B: Journal of Engineering Manufacture*, 224(10):1591–1598, Oct 2010.
31. P. Pedersen. On optimal orientation of orthotropic materials. *Structural Optimization*, 1(2):101–106, jun 1989.
32. Hardikkumar Prajapati, Darshan Ravoori, Robert L. Woods, and Ankur Jain. Measurement of anisotropic thermal conductivity and inter-layer thermal contact resistance in polymer fused deposition modeling (FDM). *Additive Manufacturing*, 21:84–90, May 2018.
33. Xiaoping Qian. Undercut and overhang angle control in topology optimization: A density gradient based integral approach. *International Journal for Numerical Methods in Engineering*, 111(3):247–272, Jul 2017.
34. Jordan R Raney, Brett G Compton, Jochen Mueller, Thomas J Ober, Kristina Shea, and Jennifer A Lewis. Rotational 3D printing of damage-tolerant composites with programmable mechanics. *Proceedings of the National Academy of Sciences*, 115(6):201715157, feb 2018.

35. Ole Sigmund. A 99 line topology optimization code written in matlab. *Structural and multidisciplinary optimization*, 21(2):120–127, 2001.
36. Raghavendra Sivapuram, Peter D. Dunning, and H. Alicia Kim. Simultaneous material and structural optimization by multiscale topology optimization. *Structural and Multidisciplinary Optimization*, 54(5):1267–1281, Nov 2016.
37. J. Stegmann and E. Lund. Discrete material optimization of general composite shell structures. *International Journal for Numerical Methods in Engineering*, 62(14):2009–2027, Feb 2005.
38. John C. Steuben, Athanasios P. Iliopoulos, and John G. Michopoulos. Implicit slicing for functionally tailored additive manufacturing. *Computer-Aided Design*, 77:107–119, Aug 2016.
39. Krishnan Suresh. A 199-line matlab code for pareto-optimal tracing in topology optimization. *Structural and Multidisciplinary Optimization*, 42(5):665–679, 2010.
40. Krister Svanberg. The method of moving asymptotes a new method for structural optimization. *International journal for numerical methods in engineering*, 24(2):359–373, 1987.
41. Erva Ulu, Emrullah Korkmaz, Kubilay Yay, O. Burak Ozdoganlar, and Levent Burak Kara. Enhancing the Structural Performance of Additively Manufactured Objects Through Build Orientation Optimization. *Journal of Mechanical Design*, 137(11):111410-1—111410-9, Oct 2015.
42. Nobuyuki Umetani and Ryan Schmidt. Cross-sectional structural analysis for 3D printing optimization. In *SIGGRAPH Asia 2013 Technical Briefs on - SA '13*, pages 1–4, New York, New York, USA, 2013. ACM Press.
43. Mark Walker and Ryan Smith. A methodology to design fibre reinforced laminated composite structures for maximum strength. *Composites Part B: Engineering*, 34(2):209–214, mar 2003.
44. Michael Yu Wang, Xiaoming Wang, and Dongming Guo. A level set method for structural topology optimization. *Computer Methods in Applied Mechanics and Engineering*, 192(1-2):227–246, Jan 2003.
45. Wikipedia contributors. Fused filament fabrication — Wikipedia, the free encyclopedia, 2018. [Online; accessed 25-May-2018].
46. Jun Wu, Anders Clausen, and Ole Sigmund. Minimum compliance topology optimization of shell-infill composites for additive manufacturing. *Computer Methods in Applied Mechanics and Engineering*, 326:358–375, Nov 2017.
47. Jun Wu, Charlie CL Wang, Xiaoting Zhang, and Rüdiger Westermann. Self-supporting rhombic infill structures for additive manufacturing. *Computer-Aided Design*, 80:32–42, 2016.
48. Yi M Xie and Grant P Steven. A simple evolutionary procedure for structural optimization. *Computers & structures*, 49(5):885–896, 1993.
49. Yi Min Xie, Zhi Hao Zuo, Xiaodong Huang, and Jian Hua Rong. Convergence of topological patterns of optimal periodic structures under multiple scales. *Structural and Multidisciplinary Optimization*, 46(1):41–50, Jul 2012.
50. Praveen Yadav and Krishnan Suresh. Assembly-Free Large-Scale Modal Analysis on the Graphics-Programmable Unit. *Journal of Computing and Information Science in Engineering*, 13(1):011003, Jan 2013.
51. Praveen Yadav and Krishnan Suresh. Large Scale Finite Element Analysis via Assembly-Free Deflated Conjugate Gradient. *Journal of Computing and Information Science in Engineering*, 14(4):041008, Oct 2014.
52. Jun Yan, Xu Guo, and Gengdong Cheng. Multi-scale concurrent material and structural design under mechanical and thermal loads. *Computational Mechanics*, 57(3):437–446, Mar 2016.
53. Pu Zhang, Jikai Liu, and Albert C. To. Role of anisotropic properties on topology optimization of additive manufactured load bearing structures. *Scripta Materialia*, 135:148–152, Jul 2017.
54. Xiaoting Zhang, Xinyi Le, Athina Panotopoulou, Emily Whiting, and Charlie CL Wang. Perceptual models of preference in 3d printing direction. *ACM Transactions on Graphics (TOG)*, 34(6):215, 2015.